Non-Fickian diffusion in biosourced materials: Experimental determination of the memory function using minute samples

A. Challansonnex, J. Casalinho, P. Perré

Non-Fickian diffusion in biosourced materials: Experimental determination of the memory function using minute samples

A. Challansonnex[a,*], J. Casalinho[a], P. Perré[a,b]

[a] *LGPM, CentraleSupélec, Université Paris-Saclay, 8-10 rue Joliot-Curie, 91 190 Gif-sur-Yvette, France*
[b] *LGPM, CentraleSupélec, Centre Européen de Biotechnologie et de Bioéconomie (CEBB), 3 rue des Rouges Terres, 51 110 Pomacle, France*

Abstract

Focusing on non-Fickian diffusion in biosourced materials, we have recently developed a new formulation that can model this behavior using memory functions. To identify those memory functions, an experimental device based on a magnetic suspension balance is used. Very thin samples of low-density fiberboard, medium-density fiberboard, and Spruce in the longitudinal direction are subjected to variations in ambient relative humidity (RH) while their mass is recorded. The imposed RH and temperature are used as boundary conditions in a comprehensive model to solve the heat and mass transfer equations in porous media. A computational code solving the new formulation was used to determine the memory functions by inverse analysis. The use of very thin samples enables macroscopic parameters to be considered as negligible compared to microscopic effects.

Keywords: Non-Fickian diffusive behavior, renewable materials, coupled transfer, experiment

1. Introduction

In the past few decades, an interest in the conception of buildings more respectful of the environment has emerged. In particular, biosourced materials offer good performances with a reduced ecological footprint. The determination of their thermal and hygroscopic characteristics is of great interest to properly model the energetic characteristics of buildings [1, 2]. However, in fibrous materials such as fiberboards, a non-Fickian diffusive behavior has been observed. This may lead to several consequences in transient modes such as a dependence of the mass diffusive coefficient on material thickness [3]. We also suspect the delay between relative humidity (RH) and moisture content that is observed in [4] to be due to this phenomenon. More generally, it has been shown that a classical formulation of coupled heat and mass transfer is unable to model the behavior of those materials [5]. This kind of behavior is due to the dual-scale nature of the material that leads to an absence of thermodynamic equilibrium [6, 7, 8, 9]. Indeed, a fiberboard panel comprises two phases with contrasting characteristics, as represented in Fig. 1(a): 1. a

*Corresponding author
Email address: arnaud.challansonnex@centralesupelec.fr (A. Challansonnex)

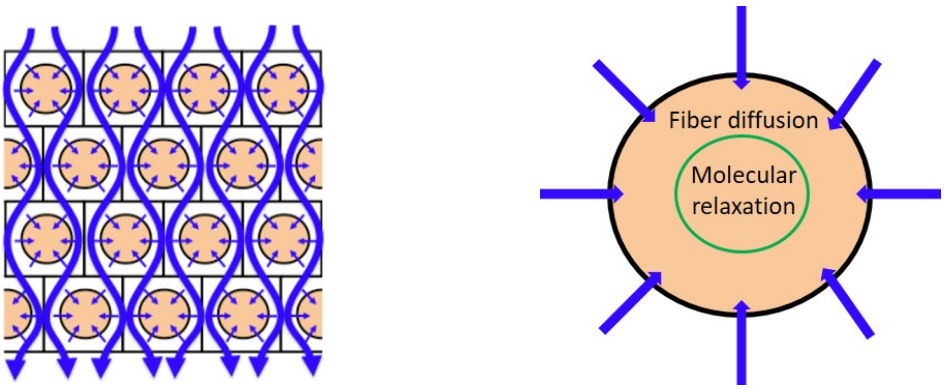

Figure 1: From left to right: (a) Schematic presenting the diffusion in a material composed of two phases with contrasted diffusivity; (b) schematic presenting the diffusion inside a fiber, with two distinct phenomena

gaseous phase, which is highly diffusive and well connected, and 2. the fibers themselves, which are weakly diffusive and poorly connected. Therefore, two time constants interfere during transient diffusion, the macroscopic time constant linked to diffusion in the gaseous phase and a microscopic time constant linked to diffusion in the fibers. The microscopic time constant being superior to or even of the same order of magnitude as the other results in the absence of thermodynamic equilibrium. This kind of behavior has also been observed in the longitudinal direction of massive wood, owing to the strong vapor diffusion inside the vessels and tracheids, which in this case constitute the gaseous phase [10].

Furthermore, one part of the fibers reacts to a perturbation of ambient RH with a much longer characteristic time than the rest of it (several tens of hours instead of a few minutes). This phenomenon is known as molecular relaxation of vegetable polymers. It can be described as a rearrangement of the molecular state when a penetrant diffuses into a polymer substance [11, 12, 13, 14, 15]. The polymer molecules must take up a new configuration to accommodate the penetrant molecules. As a consequence, a long delay for the material to reach equilibrium is created when the fibers are submitted to a variation of the ambient RH [16, 17]. As a result, as represented in Fig. 1(b), diffusion in the fibers occurs in two consecutive stages. In the following text, the short-time diffusion will be referred to as *fiber diffusion* whereas the long-time diffusion will be referred to as *molecular relaxation*.

One of the main objectives of this paper is to characterize the diffusion in the fibers at the microscopic scale. Therefore, we chose to study a configuration where microscopic effects are predominant compared to macroscopic ones. This was achieved by studying diffusion in very thin samples. Indeed, in one-dimensional diffusion, the characteristic time increases as the diffusion path thickness square. As can be observed in Fig. 2, by reducing the thickness of the sample, the macroscopic characteristic time becomes negligible compared to those of both molecular relaxation and fiber diffusion.

We have recently worked on a new formulation [18] that can model these kinds of microscopic behaviors using memory functions. This formulation will be briefly presented. Those memory functions are identified using experimental results obtained with a device built around a magnetic suspension balance. Minute samples of low-density fiberboard

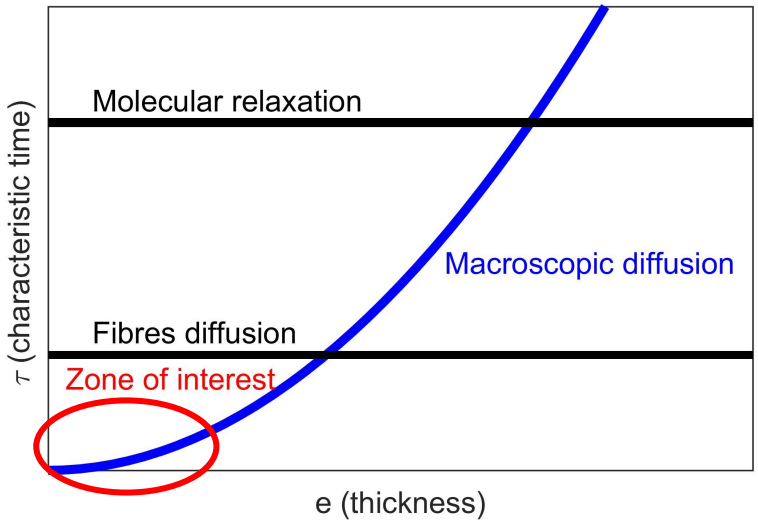

Figure 2: Drawing showing the effect of reducing the sample thickness on characteristic times

(LDF), medium-density fiberboard (MDF), and Spruce wood in the longitudinal direction were submitted to variations in ambient RH while their mass variation is measured. The data are then analyzed by using an inverse method. The model that is used is a comprehensive system of equations that takes into account the coupling between heat and mass. This system is solved using the computational code based on the finite volume method *Transpore* [19, 20], which is embedded in the optimization algorithm. The new formulation with memory effects was recently implemented in the code.

2. Materials and methods

2.1. Materials

The three materials that were studied are LDF, MDF, and Spruce wood in the longitudinal direction. For all materials, the macroscopic diffusivity was taken either from literature or from experiments performed in our lab. Note however that, as explained above (Fig. 2), the sample dimension is so small that this parameter has little effect compared to the microscopic effect.

LDF is an insulation material made of wood fibers agglomerated by their bonding properties. Its thermal and hygroscopic characteristics have already been widely studied [21, 22, 23, 24]. The sample comes from a 1-cm-thick panel with a density of 255 kg/m^3 (and note that all densities were measured at 40% RH). It is produced by Steico (Munich, Germany) and contains only wood fibers. Concerning the mass diffusivity of the material, we define the reduced mass diffusivity f as the ratio of the effective diffusivity of the material over the binary diffusivity of water vapor in air ($f = \frac{D_{eff}}{D_v}$). This coefficient was taken from literature [3] and set at 0.45.

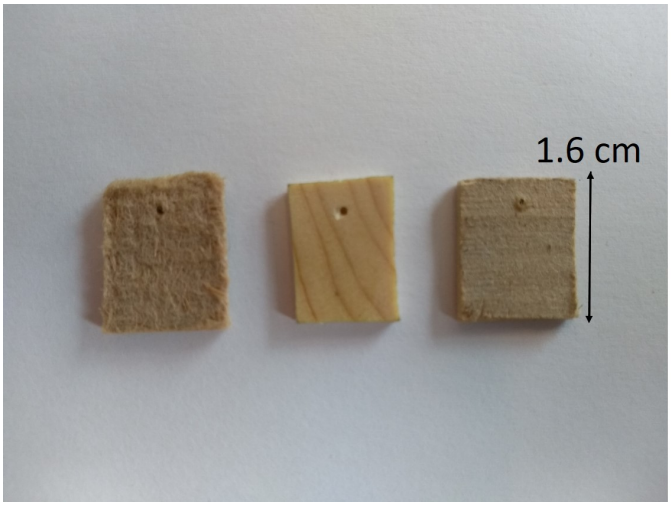

Figure 3: Photograph of the three samples, from left to right: LDF, Spruce, and MDF

MDF is a material constituted of wood fibers, urea-formaldehyde resin, and paraffin wax [25]. The panel is formed by applying high temperature and pressure. It is mostly used in interior design and decoration. Its thermal and hygroscopic characteristics have also been widely investigated [25, 26, 5]. The material that was studied comes from a 1-cm-thick panel with a density of 655 kg/m^3. Its dimensionless diffusivity f was taken from a previous studies [27] and set at 0.075.

Spruce wood is a softwood that is commonly used in building construction and whose transport characteristics have also been investigated [28, 5]. Even if in use the mass transfer does not usually occur in the longitudinal direction, it is of great interest to observe the absence of thermodynamic equilibrium in a nonfibrous material that has not undergone any modification process. The wood that was used in this work has a density of 455 kg/m^3. According to eperiments performed in our lab, its dimensionless diffusivity coefficient was set at 0.05.

Small rectangular shaped samples of 1.6 cm in length and 1.2 cm in width were cut perpendicular to the sheet plan for fiberboards and perpendicular to the board for spruce. A wire diamond saw was used to preserve the structure of the materials. A photograph of the samples can be observed in Fig. 3. The thickness of these samples was chosen to be thin enough for the microscopic effects dominate over the macroscopic effects but thick enough to maintain the macroscopic structure of the material. Therefore, LDF and Spruce samples are 1.7 mm thick and the MDF sample is 1.4 mm thick. Choosing such sample thicknesses kept the diffusive path length always <1 mm.

2.2. Experimental setup

The experimental setup is based on a suspension magnetic balance (Rubotherm-10-μg-MSB, TA Instrument, New Castle, United States). The measurement chamber is controlled in terms of RH and temperature. RH control is made via a humidity generator (MHG-32, ProUmid GmbH & Co., Ulm, Germany). The temperature is controlled with a cryothermostat (Ministat230, HUBER, Offenburg, Germany) that circulates water within

a double-wall jacket that encloses the chamber. The sample is attached to a hook connected to a permanent magnet coupled to an electromagnet that is weighed by the balance. In this manner, the electronic part can be isolated from the sample room, allowing a wide range of conditions in terms of RH and temperatures to be obtained without condensation or leakage problems. The principle of the experiment is then to submit the sample to a sudden change in ambient RH and to record its mass variation over time at a very high resolution (0.01 mg) as well as the ambient conditions inside the chamber through the RH and temperature sensors. A regular taring offers very good reproducibility ($\pm$0.02 mg). Note that, for this experiment, special care has been taken in the placement of the RH and temperature sensors. Indeed, because of the very subtle phenomena that are observed, the sensors had to be placed between the air inlet of the humidity generator and the sample, so that the sample does not perturb the RH being read by the sensor. A photograph of the experimental device can be observed in Fig. 4, and more details about it can be found in Ref. [29].

In the current experiment, samples were first dried using nitrogen flow. This allows us to obtain an anhydrous mass while avoiding hysteresis effects and thus ensures the reproducibility of the experiment. Then, four jumps in RH followed by a plateau were studied: from 0% to 20%, 20% to 40%, 40% to 60%, and 60% to 80%. During this experiment, the acquisition rate was set at 30 s and taring occurred every 5 min. A wide range of RH values were chosen because molecular relaxation depends on RH. Indeed, its effect is known to be stronger at high RH [30]. The plateau duration is a function of the relaxation observed. Our stopping criterion is a gain of $<$0.000012/h during 5 h in terms of moisture content. If this exigent criterion is not reached, the plateau is stopped after 100 h, which was the case for the highest RH (80%). All the experiments were performed under isothermal conditions at 35 °C. An example of the experimental results obtained can be observed in Fig. 5 for the first three plateaus of MDF.

2.3. Assessing the sensor drift over long durations

Molecular relaxation is characterized by a slow evolution of the moisture content toward equilibrium when the sample is submitted to a perturbation of the imposed RH. However, to ensure that such an observation is due to molecular relaxation, one must know very precisely the actual value of the surrounding RH. For that purpose, we performed an accurate calibration of our sensors over long durations. To do this, we used a dew point analyzer (Optidew, Michell Instruments, Lyon, France) as reference information, as the RH is obtained via the value of the dew point temperature (MHG sensor). In this kind of apparatus, the temperature is measured via a very stable Pt100 sensor. Two RH sensors were tested: a Sensirion SHT75 (HDI Electronics, Perois, France) and the regulation probe of the moist air generator. They were both placed in a climatic chamber (HPP110, Memmert, Schwabach, Germany) nearby the dew point transmitter. Then, similarly to what is done in the experiment, stepwise RH variations are imposed (20% to 40%, 40% to 60%, and 60% to 80%) under isothermal conditions (35 °C). Each step duration was chosen to last 50 h, as can be observed in Fig. 6(a). As can be observed in Fig. 6(b), for the step from 60% to 80%, the SHT75 sensor slowly drifts to its equilibrium value. This behavior disqualifies this sensor in this experiment and the RH value that is recorded in this work is then the value of the regulation probe, which presented no major differences in its kinetic

Figure 4: Experimental setup, showing 1: magnetic suspension balance, 2: heating jacket enclosing the measuring chamber, 3: humidity generator, and 4: cryothermostat for temperature control

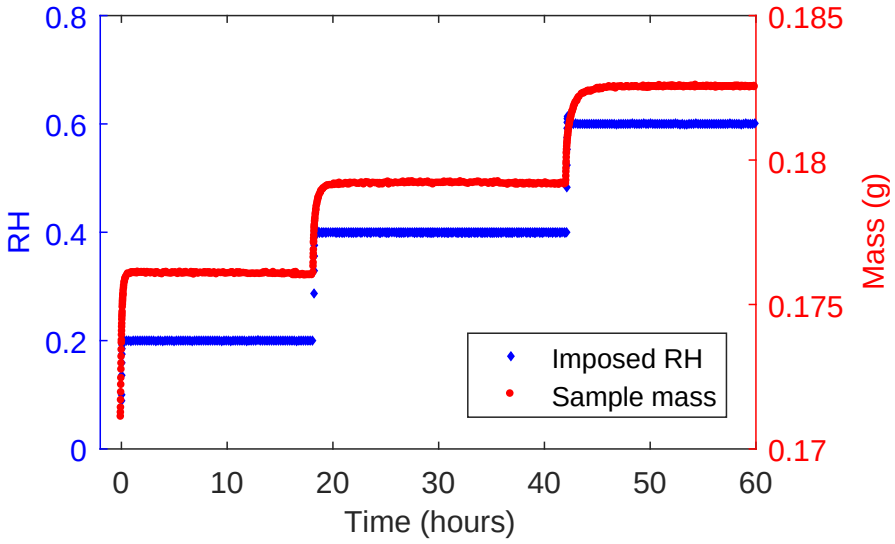

Figure 5: Evolution of sample mass and imposed RH with time for MDF during the first three plateaus

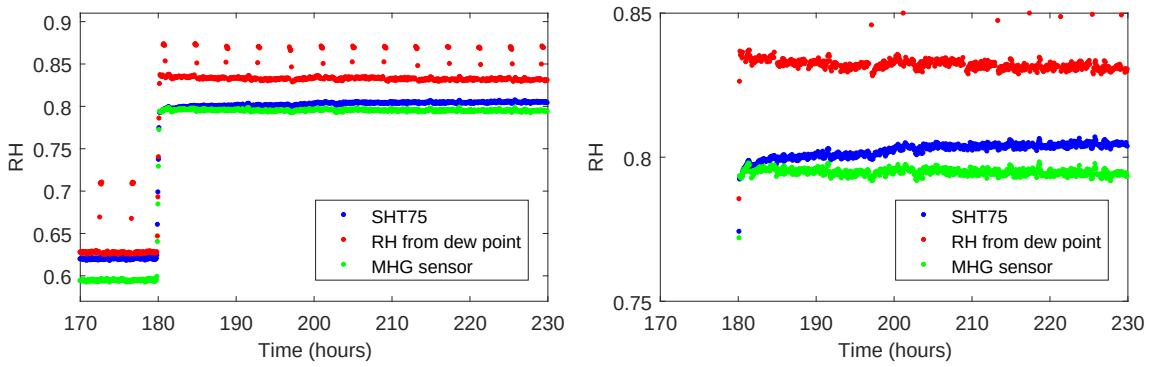

Figure 6: From left to right: (a) Experimental results for sensor testing for the 60%–80% RH jump; (b) expanded view of the RH zone of interest

behavior compared to that of the transmitter.

2.4. Measurement of the external heat transfer coefficient

Because of the small sample thickness, simulation results depend quite strongly on the external heat transfer coefficient h_h. Fortunately, this coefficient is solely controlled by the boundary layer around the sample. During drying, the heat transfer coefficient controls the drying rate during the constant drying rate period (CRP) , whatever the sample properties [31, 32] . The sole necessary conditions is the existence of a well established CRP. To measure the heat transfer coefficient, the flow conditions must be similar to the experiment. Drying tests were therefore performed in the same device for a sample of sponge of similar geometry. This allows a nice CRP to be obtain. This piece of sponge was saturated with water and then placed in the experimental device just like a sample would have been. A jump of RH from 20% to 40% was made at a temperature of 35 °C. During the CRP, the sample temperature is at the wet bulb temperature T_w, uniform in space and constant in time. No conductive heat flux exists. Consequently, the heat flux q_h supplied to the sample through the external heat transfer is entirely devoted to the latent heat of vaporisation required to ensure the drying rate q_v determined by the time-evolution of sample mass:

$$L_v q_v = q_h = S h_h (T_d - T_w), \tag{1}$$

where L_v the latent heat of vaporisation of water, q_v is the drying rate ($kg.m^{-2}.s^{-1}$) as determined by sample mass versus time during the CDR period, S is the exchange surface area, T_w is the wet bulb temperature and T_d is the dry bulb temperature.

The value of h_h, the sole unknown of equation (1), is simply determined using the experimental data. More detail about this method can be found in published works [33, 34]. A h value of 20.46 $\mathrm{W{\cdot}m^{-2}{\cdot}K^{-1}}$ was obtained, which is consistent with the air velocity and sample size. In the simulation code, the mass transfer coefficient h_m is also needed. It was determined using the analogy between heat and mass transfer assuming the Lewis number to be equal to unity:

$$h_m = \frac{h_h}{\rho_g c_{pg}}, \tag{2}$$

3. Physical model with memory effects

The physical model used in the inverse procedure is a comprehensive model that takes into account the coupling between heat and mass transfer [19, 20], even though, due to the thinness of the samples, the coupling is not so important in this work. Besides, the absence of thermodynamic equilibrium must be considered. This effect is transferred at the macroscopic scale thanks to the new formulation proposed and validated in [18].

The real morphology of a fibrous material such as LDF can be approached by a Representative Elementary Volume (REV) which consists of a set of long cylinders surrounded by a void as represented in figure 1. The relevant size of this REV was shown in previous paper to be about 500 μm [35]. Consider that the storage phase (the fibers) is submitted to a sudden change in ambient RH from RH_{ini} to RH_{fin} at t_0. If $X(t)$ is the moisture content of the storage phase, for $t < t_0$, $X(t) = X_{ini} = X_{eq}(RH_{ini})$, where $X_{eq}(RH)$ is the equilibrium moisture content value defined by the sorption isotherm.

At $t = t_0$, the boundaries of the storage phase can be considered to be at equilibrium with RH_{fin}, as the external resistance is negligible due to the very slow diffusion inside the fibers. From this instant, diffusion and molecular relaxation operate inside the fiber. The phenomenon is formulated using a memory function [18] which allows the averaged moisture content of the fiber to be expressed as follows:

$$X(t) - X_{ini} = \Delta X_{eq} \varphi(t), \tag{3}$$

where $\Delta X_{eq} = X_{eq}(RH_{fin}) - X_{eq}(RH_{ini})$ and φ is the memory function, a monotonic function that tends to unity as t tends to infinity. In order to represent diffusion inside the fibers, the analytic solution of diffusion into a cylinder can be used [36, 37]. Note that this formulation is also able to account for molecular relaxation provided an additional, larger, time constant to the memory function.

In a more general case, the RH value surrounding the fiber varies over time and a convolution product is required to account for this time dependence:

$$X(t) - X_{ini} = \int_0^t \varphi(t - \tau) \frac{\partial X_{eq}}{\partial \tau} d\tau, \tag{4}$$

where

$$\frac{\partial X_{eq}}{\partial \tau} d\tau = dX_{eq} \tag{5}$$

dX_{eq} represents the variation of equilibrium moisture content during the infinitesimal time interval $d\tau$.

To account for the memory effect, X should be used for mass balance while all driving forces involved in convective or diffusive fluxes should be tied to X_{eq} to consider the right water activity a_w. This rule stands for mass fraction, capillary pressure, moisture content, chemical potential and so on. For simplicity, the mass balance equation can be written in a compact manner, where q_m represents the total convective flux of moisture, and j_m is the total diffusive flux of moisture:

$$\rho_0 \frac{\partial X}{\partial t} + \nabla \cdot (\boldsymbol{q}_m(X_{eq})) = \nabla \cdot (\boldsymbol{j}_m(X_{eq})) \tag{6}$$

Considering that the moisture mass in the gaseous phase is negligible compare to that of the storage phase, we can define X as the average moisture content over the microstructures. Thus, by combining (4) and (6) we obtain a new equation involving only X_{eq}:

$$\frac{\partial}{\partial t}\left(\int_0^t \varphi(t-\tau)\frac{\partial X_{eq}}{\partial \tau}d\tau\right) + \nabla\cdot(\boldsymbol{q}_m(X_{eq})) = \nabla\cdot(\boldsymbol{j}_m(X_{eq})) \tag{7}$$

In equation (7), the convolution product defines implicitly the relationship between X and X_{eq} at any time and for each point in the domain. This convolution product can be solved easily when the memory function is of the form $\varphi(t) = 1 - \sum_{i=1}^{N}\alpha_i \exp(-\frac{t}{\tau_i})$. This decomposition allows us to implement each exponential function in the computational code as an internal variable that is updated at each node of the computational domain using the evolution of dX over each time increment. Thanks to these internal variables, a simple relation relies X and X_{eq} (see the appendix). This is a quite common way to deal with convolution product, for example to deal with viscoelasticity [38, 39, 40]. A recent paper proposes also this solution, for a 1-variable model, for fading memory for dual scale transport in porous media [41]. In our case, equation (7) is embedded in the full system of heat and mass transfer macroscopic equations (three balance equations with three state variables) that is solved by the computational code *TransPore*. For greater clarity, the full set of equations, as defined in [18], is detailed in the appendix, where the indice $_{eq}$ indicates that the corresponding value should be calculated using X_{eq} instead of X.

4. Data analysis

4.1. Chosen form of the memory function

In practice, the memory function can always be approached as a sum of exponential functions. For example, it is proved in Ref. [18] that the analytical solution of diffusion into fibers (an infinite sum of exponential functions) can be, surprisingly, approached by only one or two exponential functions. In addition, it was shown in the same work that two phenomena arising at different spatial scales (molecular relaxation and diffusion inside fibers) can still nicely approach the sum of two exponential functions at the macroscopic scale, as long as the characteristic times of the two phenomena are significantly different. Subsequently, we have chosen here to define φ by the sum of two exponential functions: one for dual-scale diffusion (φ_{fd}) and one for molecular relaxation (φ_{mr}). Therefore, we have $\varphi = 1 - \varphi_{fd} - \varphi_{mr}$, with $\varphi_{fd} = \alpha_{fd}\exp(-\frac{t}{\tau_{fd}})$ and $\varphi_{mr} = \alpha_{mr}\exp(-\frac{t}{\tau_{mr}})$.

4.2. Inverse procedure

The principle of identification is to feed the physical model with known sample characteristics (thickness, density, porosity, diffusion coefficient, thermal conductivity, etc.) and estimated values of the unknown parameters (the parameters introduced above, i.e. the set α and τ for each exponential function). The physical model uses a 3-variable formulation of coupled heat, mass and momentum transfer in porous media [20]. All measured parameters such as the external heat transfer coefficient, as explained in section 2.4 and the sorption isotherm are also supplied to the code, hence are not part of the identified parameters. We made this choice intentionally to get more relevance to the identified parameters and avoid

the algorithm to be trapped in local minima. As we know the anhydrous mass of each sample from our experiment, the sorption isotherm is determined directly from the experimental data. By using the recorded conditions of the chamber (RH and temperature) as boundary conditions, the computational code is able to predict the mean moisture content of the sample. An objective function S quantifies the difference between the predicted and experimental values of the mean moisture content as a sum of the square residues. This function has the following form:

$$S = \sum_{i=1}^{N} w_i [X_{exp}(t_i) - X_{pred}(t_i)]^2, \tag{8}$$

where X_{exp} is the experimental value, X_{pred} is the predicted value, t is time, N is the number of time intervals, and w_i is the weighting factor, which is proportional to the time interval (where here the time interval does not vary).

The unknown parameters are modified by an optimization algorithm (downhill Simplex [42]) that iterates to minimize the objective function. The parameters α and τ are thus obtained after convergence.

4.3. Identification strategy and sensitivity analysis

One of the main difficulties of this work is separating the contributions of fiber diffusion and molecular relaxation. However, because the characteristic times of the two phenomena are supposed to be very different, the effect of fiber diffusion should be predominant during the first instants after the perturbation whereas molecular relaxation should be predominant for long-time diffusion [43]. The strategy adopted will be illustrated in Fig. 7 for the case of the jump between 40% and 60% RH for LDF. In Fig. 7(a), one can observe the set of experimental data (imposed RH and sample moisture content) during the whole acquisition.

The first step consists of identifying α_{fd} and τ_{fd} over a period that lasts one hour after the RH perturbation. Therefore, one considers that during this period the only contribution is due to fiber diffusion, whose parameters are identified, while molecular relaxation parameters are set to zero. This step can be observed in Fig. 7(b). One can see that the model has a particular shape during the very first instants after the perturbation. Indeed, the curve shows an inflection point. This is due to the imposed RH that is used as a boundary for the model. Actually, one can see in Fig. 7(a) that it is not a perfect Heaviside function but that there is a slight overshoot of the targeted RH.

In the second step, α_{mr} and τ_{mr} are identified over the whole acquisition. The effects of both phenomena are considered, with the values of the fiber diffusion parameters being fixed at the values found before. This step can be observed in Fig. 7(c).

Finally, the third step consists of adjusting the parameters by identifying their four values at the same time over the whole acquisition using the values found in the first two steps as starting points. This last step can be observed in Fig. 7(d). In this figure, one can also observe the behavior of the model if the time constants were null, that is, for a classic formulation without memory functions. In this case, the model is far too fast and does not capture the kinetics of the transfer. One can also observe that there is a slight overshoot because of the value of imposed RH. For this last step, the identified values were $\alpha_{fd} = 0.38$, $\tau_{fd} = 3.2 \times 10^3$ s, $\alpha_{mr} = 0.13$, and $\tau_{mr} = 2.6 \times 10^4$ s.

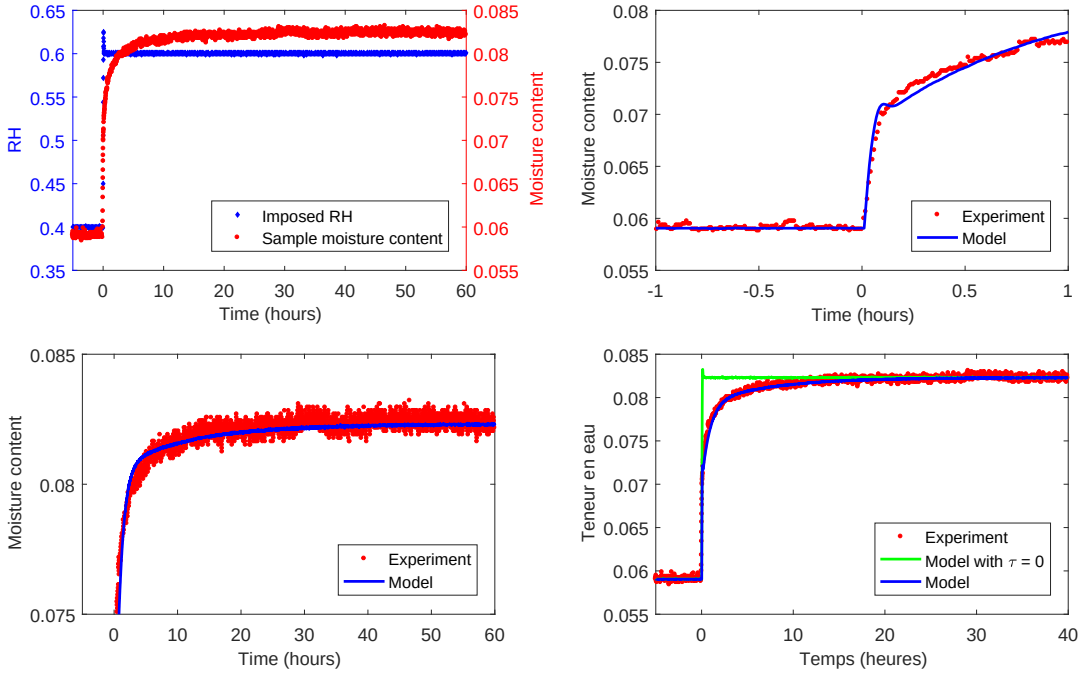

Figure 7: From left to right and top to bottom: (a) Experimental evolution of the moisture content for LDF for the 40%–60% jump % and imposed RH, (b) identification of the first exponential function at short times, (c) identification of the second exponential function at long times, and (d) final identification

To check whether the identified parameters were really independent, a sensitivity analysis was performed. For each parameter β, two consecutive simulations were done: one with parameter β fixed at its identified value ($\beta = \beta_0$) and one with $\beta = \beta_0(1+\epsilon)$, where $\epsilon = 10^{-2}$. Other parameters were kept at their identified values. One can then obtain the profile over the whole step duration of the relative variation of the moisture content with respect to each parameter:

$$\frac{X(t)_{\beta=\beta_0(1+\epsilon)} - X(t)_{\beta=\beta_0}}{\epsilon X(t)_{\beta=\beta_0}}. \tag{9}$$

The evolution of the sensitivity coefficients over the entire range of a sorption test are presented in Fig. 8. One can note the following:

- Parameters α has a strong influence at very short times because the proportion of the storage phase that does not react with a relaxation time $(1 - \alpha_{fd} - \alpha_{mr})$ reacts immediately. Consequently, for each exponential function, the amplitude α and time constant τ affects the answer over different times scales, which proves that these coefficients are independent.

- Similarly, owing to the contrast in time constants for the two exponential functions, one can also confirm that the two sets of parameters are independent, which validates our identification strategy.

The strategy of the present work is to use minute samples to focus the experimental data on microscopic effects. To confirm this assumption, the same procedure was applied with

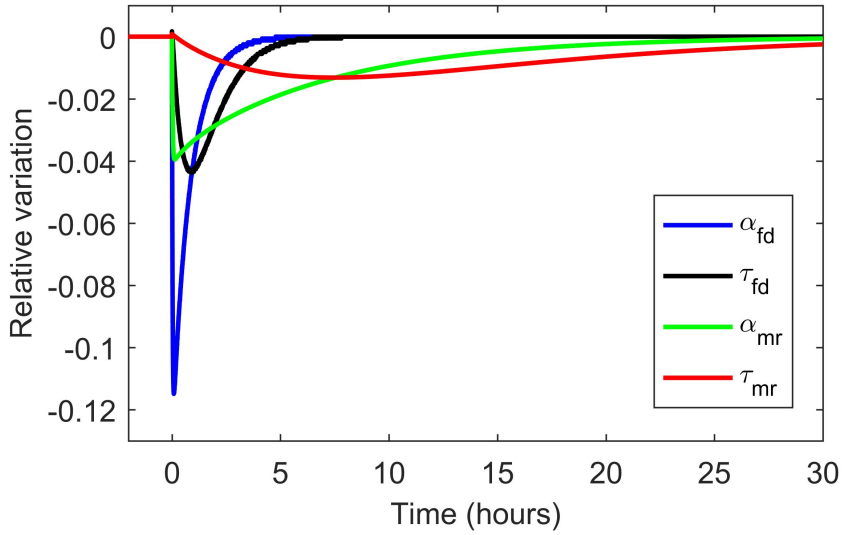

Figure 8: Sensitivity of moisture content to the identified parameters for the jump in RH from 40% to 60% for LDF

the dimensionless diffusivity coefficient (Fig. 9). The peak of the influence of this parameter is very small (5×10^{-3}) and is reached during the first minutes after the perturbation: After 10 min, its value is already negligible. Those observations confirm what was observable in Fig. 7(d): that the dimensionless diffusivity coefficient has an influence on very short times that is not representative of the behavior of the material. This demonstrates that the influence of the macroscopic diffusivity on the identification of microscopic parameters is completely negligible.

5. Results and discussion

5.1. Identification of the memory functions

Jumps in RH (%)	α_{fd}	τ_{fd} (s)	α_{mr}	τ_{mr} (s)
0–20	0.80	1.7×10^2		
20–40	0.30	1.0×10^3	0.10	1.1×10^4
40–60	0.38	3.2×10^3	0.13	2.6×10^4
60–80	0.52	3.1×10^3	0.07	1.3×10^5

Table 1: Identified coefficients for LDF

Figure 10 presents the experimental simulated curves, after identification, for the four RH steps imposed on the LDF sample. These results are also summarized in Table 1. The agreement between the model and the experiment is very good for every step. As expected, for the jump in RH from 0% to 20% (Fig. 10(a)), a single short relaxation time is needed to fit the experiment. The identified characteristic time (τ_{fd}) is ~3 min and its proportion (α_{fd}) is close to one, which seems to prove that the surrounding effect behind

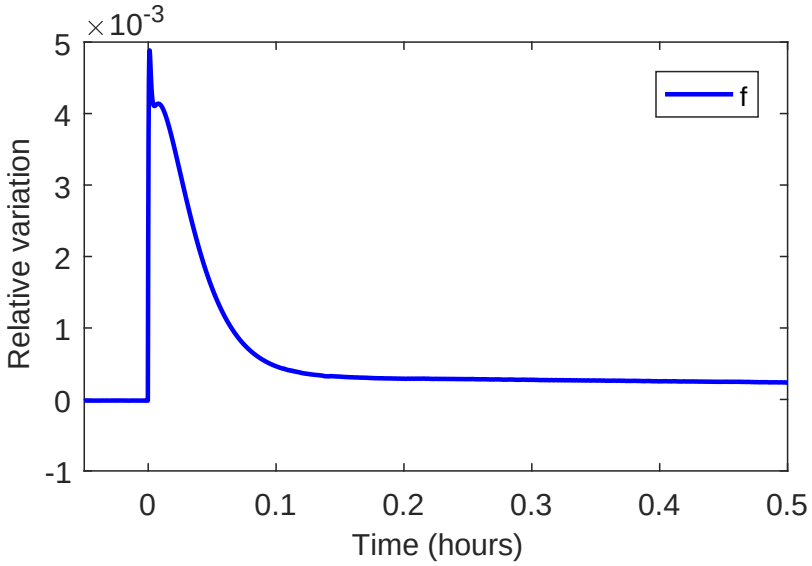

Figure 9: Sensitivity of moisture content to the macroscopic diffusive coefficient for the jump in RH from 40% to 60% for LDF

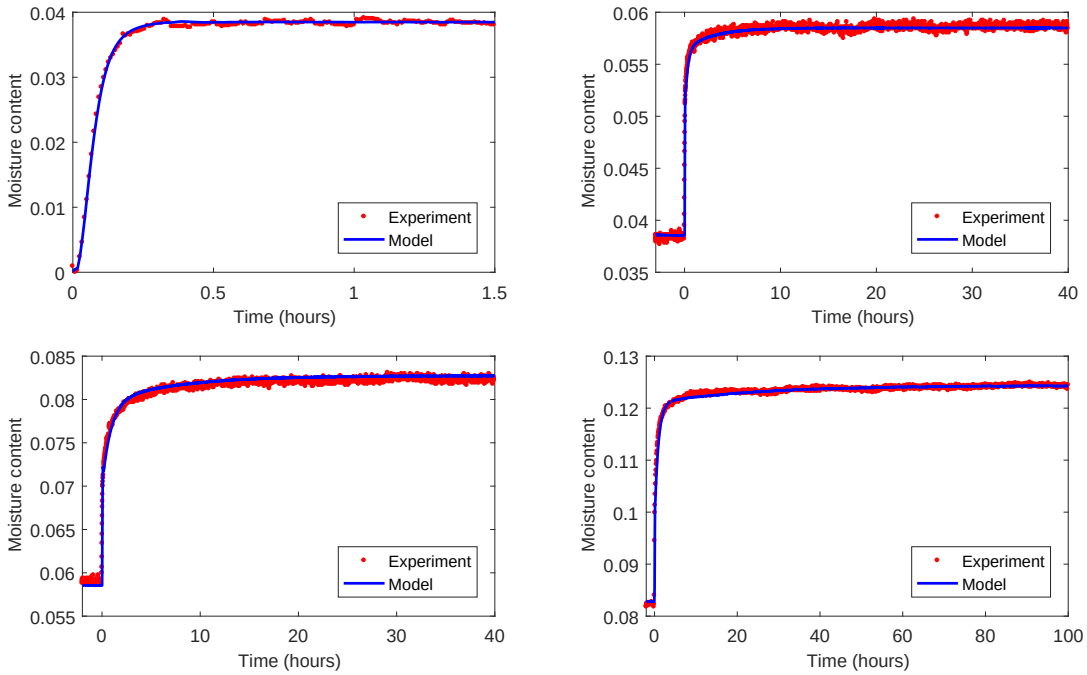

Figure 10: From left to right and top to bottom: Identification for LDF during stepwise RH from (a) 0% to 20%, (b) 20% to 40%, (c) 40% to 60%, and (d) 60% to 80%

this function is diffusion in fibers. For the jumps in RH from 20% to 40% and 40% to 60% (Figs. 10(b) and 10(c)), two exponential functions were required to fit the experimental results. The short characteristic times were ∼17 min for the 20%–40% jump and 50 min for the 40%–60% jump. The proportions of short-time relaxation were 0.3 for the 20%–40% jump and 0.38 for the 40%–60% jump. For the long-time relaxation, the characteristic times identified were ∼3 h for the 20%–40% jump and 7 h for the 40%–60% jump with proportions of 0.10 and 0.13, respectively. We note an increase in the long characteristic time with RH, which was expected for molecular relaxation. However, the characteristic time linked with fiber diffusion also increases with RH, whereas it was expected to decrease. Indeed, several published works reported that bound water diffusion in wood increases with moisture content [44, 45]. The inverse procedure uses the degrees of freedom available with only two exponential functions to obtain the minimum value of the objective function. We believe that this could force the first function (the one having the shortest characteristic time) to account partly for diffusion inside the fibers (dual-scale mechanisms) and partly for molecular relaxation. This would also explain why the proportion α_{fd} is close to one for the 0%–20% jump and not for others. It is only for this jump that the first exponential function captures overwhelmingly the classic diffusive behavior. For the RH jump from 60% to 80%, the short characteristic time is very close to the previous ones, whereas the long characteristic time is much longer (∼36 h). In all cases, the sum of these two functions is likely to well represent the time evolution of moisture content and hence can be used for prediction in a macroscopic coupled model.

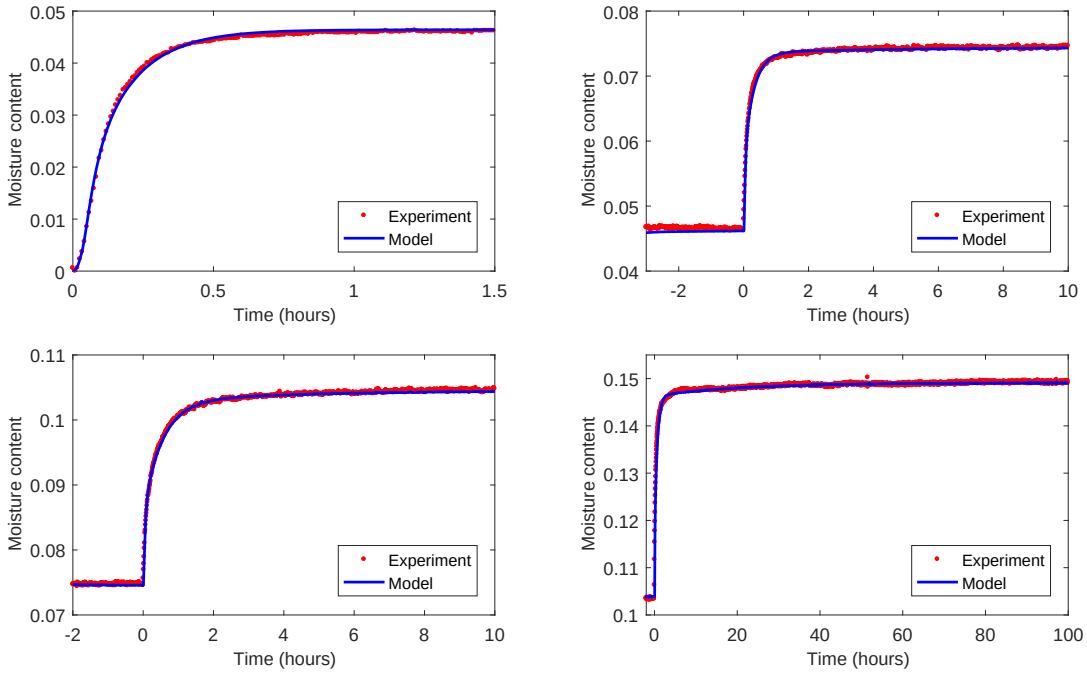

Figure 11: From left to right and top to bottom: Identification for spruce during stepwise RH from (a) 0% to 20%, (b) 20% to 40%, (c) 40% to 60%, and (d) 60% to 80%

For Spruce wood, experimental and simulated results for each jump in RH are plotted in

Jumps in RH (%)	α_{fd}	τ_{fd} (s)	α_{mr}	τ_{mr} (s)
0–20	0.45	4.2×10^2		
20–40	0.41	9.4×10^2	0.02	1.2×10^4
40–60	0.44	1.7×10^3	0.06	1.4×10^4
60–80	0.49	1.5×10^3	0.06	1.1×10^5

Table 2: Identified coefficients for Spruce

Fig. 11 and summarized in Table 2. For the short characteristic times, the proportions are similar for each step (varying from 0.41 to 0.49). Similarly to what is seen in LDF, the short characteristic times tend to rise with moisture content up to 60% (7, 15, 28, and 23 min); again, there is no need for a second exponential function for the 0%–20% jump. However, the values of those time constants are about half of those found for LDF for the 40%–60% and 60%–80% RH jumps. For the second exponential function, the long characteristic times are close to the ones found for LDF, whereas their proportions are lower. These observations seem to be consistent with the fact that, during the manufacturing of LDF (wet process), high temperatures (∼200 °C) are reached [46]. Indeed, it has been shown that thermally modified wood has a more important non-Fickian diffusive behavior tied to molecular relaxation [16].

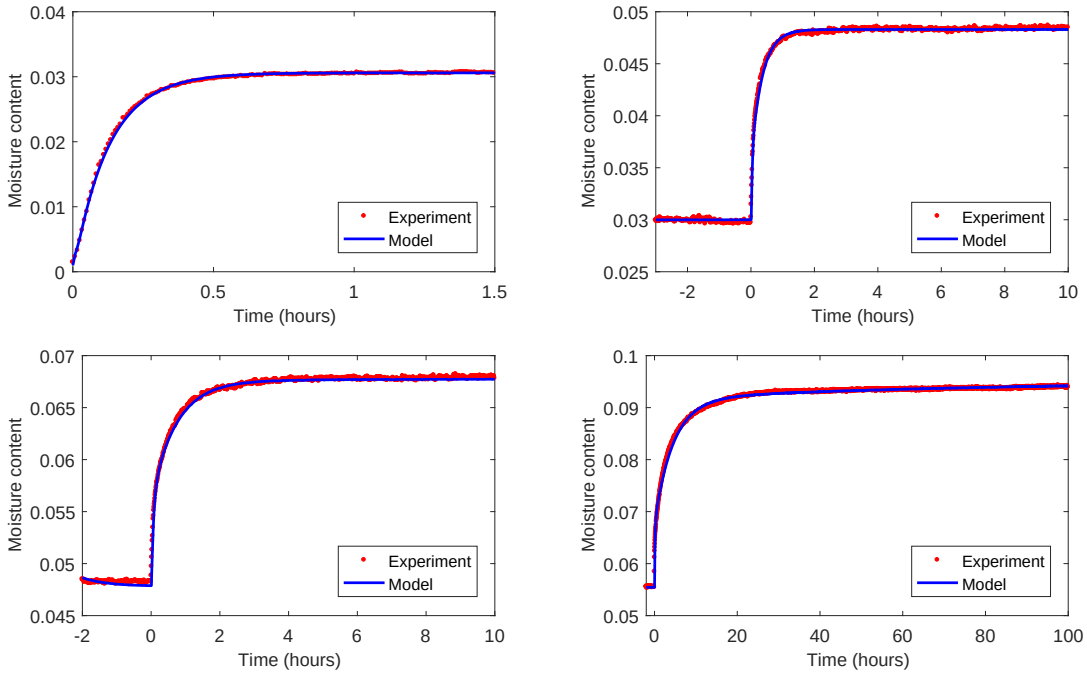

Figure 12: From left to right and top to bottom: Identification for MDF during stepwise RH from (a) 0% to 20%, (b) 20% to 40%, (c) 40% to 60%, and (d) 60% to 80%

The results for MDF can be observed in Fig. 12 and are summarized in Table 3. MDF is quite different from the two previous materials:

- Its macroscopic diffusive coefficient is lower by almost one order of magnitude, and

Jumps in RH (%)	α_{fd}	τ_{fd} (s)	α_{mr}	τ_{mr} (s)
0–20	0.71	2.8×10^2		
20–40	0.58	1.1×10^3		
40–60	0.45	2.3×10^3	0.02	4.1×10^4
60–80	0.58	1.5×10^4	0.08	3.0×10^5

Table 3: Identified coefficients for MDF

- it contains resin and wax in addition to wood fibers.

The first three jumps in RH are quite similar to those in other materials. For the jump in RH from 0% to 20%, a characteristic time of ∼5 min is found. Jumps from 20% to 40% and 40% to 60% are also similar, with short characteristic times of ∼20 and ∼50 min. A long-time relaxation is needed to fit with the experimental data only for the 40%–60% stepwise change. Finally, for the 60%–80% RH jump, the short relaxation time is much higher than the previous one (∼4 h). This difference in the diffusive behavior is clearly observable when comparing Figs. 12(c) and 12(d). During the 40%–60% jump, it took <1 h for the mass to reach 60% of its asymptotic value, whereas for the 60%–80% jump, it took >3 h to reach 60% of the final value. Because no comparable observation was done on LDF and Spruce, this fact is likely to be due to the presence of resin, which might be more prone to molecular relaxation. A second exponential function is needed to fit the experiment. Its proportion is similar to what was found for previous materials (0.08) but its characteristic time is much higher (83 h).

5.2. Identification of the diffusive coefficient of the fibers

Experimental observation of LDF done with environmental scanning electron microscopy (Fig. 13) has shown that the fibers are preferentially oriented in planes parallel to the face of the fiberboard and that their average radius is ∼20 μm. Therefore, the medium can be modeled by infinite cylinders perpendicular to the macroscopic diffusive path (similar to what can be observed in Fig. 1(a)). The moisture diffusion inside the fibers can thus be reduced to a two-dimensional problem (similar to what can be observed in Fig. 1(b)). The analytic solution corresponding to the average moisture inside the cylinder is known [47]. As stated before, this solution corresponds to the memory function φ, and thus one has

$$\varphi = 1 - \sum_{n=1}^{\infty} \frac{4}{a^2 \beta_n^2} \exp(-D_{micro} \beta_n^2 t), \tag{10}$$

where D_{micro} is the microscopic diffusive coefficient of the fibers, a is the radius of a fiber, t is time, and β_n is defined such that $a\beta_n$ is the nth root of the Bessel function of order zero.

By using φ_{fd}, the exponential function tied to fiber diffusion identified for the jump of ambient RH from 0% to 20% for LDF, it is thus possible to identify D_{micro}.

The identification procedure also uses the downhill Simplex algorithm. The number of terms, n, for the analytic solution was chosen at 500 and the roots β_n were found using an algorithm based on Halley's method. The identified value is $D_{micro} = 3.14 \times 10^{-13}$ m^2·s^{-1}. This value is close to what was found in Ref. [43].

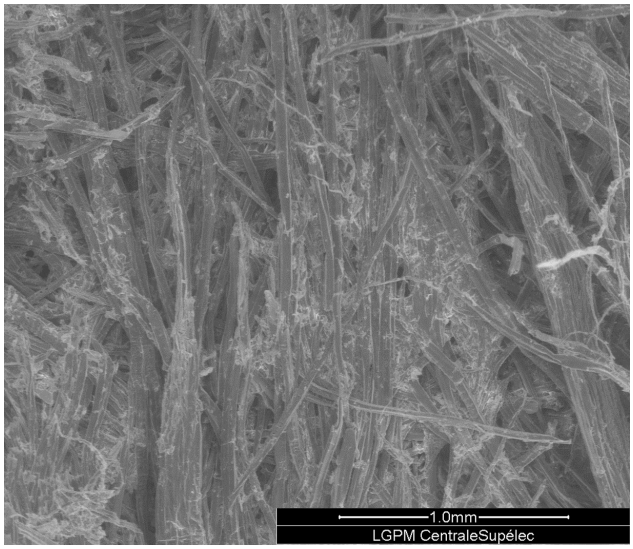

Figure 13: ESEM image of LDF

6. Conclusion and perspectives

This work focuses on non-Fickian diffusion in biosourced materials. A recently developed formulation that can model this phenomenon through memory functions has been implemented in the computational code *Transpore* [18]. This code was used as physical model in an inverse procedure to identify those memory functions for LDF, MDF, and Spruce wood in longitudinal direction. To do so, minute samples were submitted to RH variations while their masses were recorded. The following conclusions can be drawn from this work:

- The new formulation is able to capture the physics of the transfer inside those materials whereas the classic diffusive model fails.
- As confirmed by simulations and a sensitivity analysis, when using thin samples microscopic effects dominate over macroscopic effects.
- The microscopic diffusive coefficient of wood fibers can be identified.
- The effect of molecular relaxation is very different from one material to the other.

The identified memory functions could be used to predict the behavior of thicker samples. This would confirm that those functions only characterize the microscopic behavior of the material. In particular, we would like to check whether the formulation fed with those memory functions is able to predict the delay between RH and moisture content induced by the absence of thermodynamic equilibrium. A new experimental device is currently being developed to answer this question.

References

[1] H. Kunzel, A. Holm, D. Zirkelbach, A. Karagiozis, Simulation of indoor temperature and humidity conditions including hygrothermal interactions with the building envelope, Solar Energy 78 (4) (2005) 554–561. doi:10.1016/j.solener.2004.03.002.

[2] J. Jacques, M. Labat, M. Woloszyn, Dynamic coupling between vapour and heat transfer in wall assemblies : Analysis of measurements achieved under real climate, Building and Environment 87 (2015) 129–141. doi:10.1016/j.buildenv.2015.01.022.

[3] R. Rémond, G. Almeida, Mass diffusivity of low-density fibreboard determined under steady- and unsteady-state conditions : Evidence of dual-scale mechanisms in the diffusion, Wood Material Science and Engineering 6:1-2 (2011) 23–33. doi:10.1080/17480272.2010.515035.

[4] D. Lelievre, T. Colinart, P. Glouannec, Hygrothermal behavior of bio-based building materials including hysteresis effects: Experimental and numerical analyses, Energy and Buildings 84 (2014) 617–627. doi:10.1016/j.enbuild.2014.09.013.

[5] P. Perré, F. Pierre, J. Casalinho, M. Ayouz, Determination of the Mass Diffusion Coefficient Based on the Relative Humidity Measured at the Back Face of the Sample during Unsteady Regimes, Drying Technology 33:9 (2015) 1068–1075. doi:10.1080/07373937.2014.982253.

[6] K. Krabbenhoft, L. Damkilde, Double porosity models for the description of water infiltration in wood, Wood Science and Technology 38 (2004) 641–659. doi:10.1007/s00226-004-0253-5.

[7] U. Nyman, P. J. Gustafsson, B. Johannesson, R. Hägglund, A numerical method for the evaluation of non-linear transient moisture flow in cellulosic materials, International Journal for Numerical Methods in Engineering 66 (2006) 1859–1883. doi:10.1002/nme.1597.

[8] P. Perré, Multiscale Modeling of Drying as a Powerful Extension of the Macroscopic Approach: Application to Solid Wood and Biomass Processing, Drying Technology 28 (8) (2010) 944–959. doi:Doi 10.1080/07373937.2010.497079.

[9] P. Perré, Multiscale aspects of heat and mass transfer during drying, Transport in Porous Media 66 (1-2) (2007) 59–76. doi:10.1007/s11242-006-9022-2.

[10] E. Agoua, Diffusivité et perméabilité du bois: validation de méthodologies expérimentales et prise en compte de parametres morphologiques simples, Ph.D. thesis, ENGREF Nancy (2001).

[11] E. T. Engelund, L. G. Thygesen, S. Svensson, C. A. Hill, A critical discussion of the physics of wood-water interactions, Wood Science and Technology 47 (1) (2013) 141–161. doi:10.1007/s00226-012-0514-7.

[12] C. A. S. Hill, Y. Xie, The dynamic water vapour sorption properties of natural fibres and viscoelastic behaviour of the cell wall: Is there a link between sorption kinetics and hysteresis?, Journal of Materials Science 46 (11) (2011) 3738–3748. doi:10.1007/s10853-011-5286-1.

[13] L. Wadsö, Describing non-Fickian water-vapour sorption in wood, Journal of Materials Science 29 (9) (1994) 2367–2372. doi:10.1007/BF00363428.

[14] G. Christensen, Sorption and Swelling within Wood Cell Walls, Nature 213 (1967) 782–784.

[15] J. Crank, A theoretical investigation of the influence of molecular relaxation and internal stress on diffusion in polymers, Journal of Polymer Science 11 (2) (1953) 151–168. doi:10.1002/pol.1953.120110206.

[16] W. Olek, R. Rémond, J. Weres, P. Perré, Non-Fickian moisture diffusion in thermally modified beech wood analyzed by the inverse method, International Journal of Thermal Sciences 109 (2016) 291–298. doi:10.1016/j.ijthermalsci.2016.06.023.

[17] H. Håkansson, Retarded sorption in wood: Experimental study, analyses and modelling, Ph.D. thesis, Lund University (1998).

[18] P. Perré, Coupled heat and mass transfer in biosourced porous media without local equilibrium: a macroscopic formulation tailored to computational simulation, International Journal of Heat and Mass Transfer 140 (717–730).

[19] P. Perré, The Proper Use of Mass Diffusion Equations in Drying Modeling : Introducing the Drying Intensity Number, Drying Technology 33 (15-16) (2015) 1949–1962. doi:10.1080/07373937.2015.1076836.

[20] P. Perré, I. W. Turner, A 3-D version of TransPore: a comprehensive heat and mass transfer computational model for simulating the drying of porous media, International Journal of Heat and Mass Transfer 42 (24) (1999) 4501–4521. doi:10.1016/S0017-9310(99)00098-8.

[21] T. Kawasaki, M. Zhang, S. Kawai, Manufacture and properties of ultra-low-density fiberboard, Journal of wood sciences 44 (1998) 354–360.

[22] Ł. Czajkowski, W. Olek, J. Weres, R. Guzenda, Thermal properties of wood-based panels : specific heat determination, Wood Science and Technology 50 (3) (2016) 537–545. doi:10.1007/s00226-016-0803-7.

[23] J. Lux, A. Ahmadi, C. Gobbe, C. Delisée, Macroscopic thermal properties of real fibrous materials : Volume averaging method and 3D image analysis, International Journal of Heat and Mass Transfer 49 (2006) 1958–1973. doi:10.1016/j.ijheatmasstransfer.2005.09.038.

[24] O. Vololonirina, M. Coutand, B. Perrin, Characterization of hygrothermal properties of wood-based products - Impact of moisture content and temperature, Construction and Building Materials 63 (2014) 223–233. doi:10.1016/j.conbuildmat.2014.04.014.

[25] S. Ganev, R. Beauregard, G. Gendron, Effect of pannel moisture content and density on moisture movement in MDF, Wood and Fiber Science 35 (1) (2003) 68–82.

[26] W. Sonderegger, P. Niemz, Thermal conductivity and water vapour transmission properties of wood-based materials, European Journal of Wood and Wood Products 67 (3) (2009) 313–321. doi:10.1007/s00107-008-0304-y.

[27] A. Challansonnex, F. Pierre, J. Casalinho, P. Lv, P. Perré, Mass diffusivity determination of various building materials based on inverse analysis of relative humidity evolution at the back face of a sample, Construction and Building Materials 193 (2018) 539 – 546.

[28] J. Siau, Transport Processes in Wood, Springer-Verlag, 1984.

[29] G. Almeida, J. P. Lancha, F. Pierre, J. Casalinho, P. Perré, Physical behavior of highly deformable products during convective drying assessed by a new experimental device, Drying Technology 35 (8) (2017) 906–917. doi:10.1080/07373937.2016.1233883.

[30] Lars Wadsö, Measurements of water vapour sorption in wood, Wood Science and Technology 28 (1993) 59–65. doi:10.1007/BF00193877.

[31] P. Perré, How to Get a Relevant Material Model for Wood Drying Simulation ?, in: Proceeding of the first WorkShop of COST Action E 15, Edinbourgh, Scotland, 1999, pp. 1–34.

[32] P. Perré, B. May, The existence of a first drying stage for potato proved by two independent methods, Journal of Food Engineering 78 (4) (2007) 1134–1140. doi:10.1016/j.jfoodeng.2005.12.025.

[33] J. Colin, R. Rémond, P. Perré, Design and optimization of industrial woody biomass pretreatment addressed by drykiln CRP, a multiscale computational model: Particle, bed and dryer levels, Drying Technology 34 (2016) 1820–1830.

[34] P. Perré, A. Challansonnex, J. Colin, On the importance of heat and mass transfer coupling for the characterization of hygroscopic insulation materials, International Journal of Heat and Mass Transfer 133 (2019) 968–975.

[35] M. Louerat, M. Ayouz, P. Perré, Heat and moisture diffusion in spruce and wood panels computed from 3-D morphologies using the Lattice Boltzmann method, International Journal of Thermal Sciences 130 (2018) 471–483. doi:10.1016/j.ijthermalsci.2018.05.009.

[36] M. Peszynska, Fluid Flow Through Fissured Media. Mathematical Analysis and Numerical Approach, Ph.D. thesis, University of Ausburg (1992).

[37] J. Crank, The mathematics of diffusion, Oxford University Press, 1975.

[38] Simo JC; Hughes TJR, Computational Inelasticity, Springer-Verlag, 1998.

[39] B. Mauget, P. Perré, A large displacement formulation for anisotropic constitutive laws, European Journal of Mechanics - A/Solids 18 (1999) 859–877.

[40] J. Passard, P. Perré, Viscoelastic behaviour of green wood across the grain. Part II. A temperature dependent constitutive model defined by inverse method, Annals of Forest Science 62 (8) (2005) 823–830.

[41] L. Brassart, L. Stainier, Effective transient behaviour of heterogeneous media in diffusion problems with a large contrast in the phase diffusivities, Journal of the Mechanics and Physics of Solids 124 (2019) 366–391.

[42] J. A. Nelder, R. Mead, The Downhill Simplex Algorithm, Computer Journal 7 (S 308).

[43] G. Almeida, R. Remond, P. Perré, Evidence of Dual-Scale Diffusion Mechanisms in Low Density Fibreboards : Experiment and Multiscale Modelling, in: Proceedings of the 17th International Drying Symposium, Magdeburg, 2010, pp. 1023–1030.

[44] S. Avramidis, J. F. Siau, An investigation of the external and internal resistance to moisture diffusion in wood, Wood Science and Technology 21 (3) (1987) 249–256. doi:10.1007/BF00351396.

[45] A. J. Stamm, Bound-water diffusion into wood in the fiber direction, Forest Product Journal 9 (1959) 27–32.

[46] O. Suchsland, G. E. Woodson, Fiberboard manufacturing Practices In the United States, U.S. Government printing office, 1986.

[47] H. S. Carslaw, J. C. Jaeger, Conduction of heat in solids, Oxford Science Publications, 1959.

7. Appendix

The full set of equations used in the inverse procedure is detailed hereafter with two simplifications allowed by the configurations of interest: absence of liquid water (the samples are always in the hygroscopic range) and negligible macroscopic flux of bound water (water vapour diffusion always dominates at the macroscopic phase for the material chosen in this study). Indices $_{eq}$ indicate that the corresponding value should be calculated using X_{eq} instead of X. The interested reader can refer to [18] for a detailed explanation of how this new formulation was derived and to have the more general set of equations. The notations are summarized in tables 4 to 6.

Moisture conservation

$$\rho_0 \frac{\partial X}{\partial t} + \nabla \cdot (\rho_v \bar{\boldsymbol{v}}_g) = \nabla \cdot (\rho_g \boldsymbol{f} \boldsymbol{D}_v \nabla \omega_{v,eq}) \tag{11}$$

Energy conservation

$$\begin{aligned} \frac{\partial}{\partial t} \left(\varepsilon_g (\rho_v h_v + \rho_a h_a) + \overline{\rho_b h_b} + \varepsilon_s \rho_s h_s \right) \\ + \nabla \cdot ((\rho_w h_v + \rho_a h_a) \bar{\boldsymbol{v}}_g) \\ = \nabla \cdot (\boldsymbol{\lambda}_{eff} \nabla T + (h_v - h_a) \rho_g \boldsymbol{f} \boldsymbol{D}_v \nabla \omega_{v,eq}) \end{aligned} \tag{12}$$

Air conservation

$$\frac{\partial (\varepsilon_g \rho_a)}{\partial t} + \nabla \cdot (\rho_a \bar{\boldsymbol{v}}_g) = \nabla \cdot (\rho_g \boldsymbol{f} \boldsymbol{D}_v \nabla \omega_a) \tag{13}$$

Non local equilibrium

$$\begin{aligned} X_{eq}(\boldsymbol{x}, t) &= X(\boldsymbol{x}, t) + \sum_i \phi_i(\boldsymbol{x}, t) \\ \omega_{v,eq} &= \omega_v(a_w(X_{eq}, T)) \end{aligned} \tag{14}$$

Updating memory effects

$$\begin{aligned} d\phi_i &= (exp(-dt/\tau_i) - 1)\, \phi_i + \alpha_i\, dX_{eq} \\ \text{with} \quad dX_{eq} &= \frac{dX + \sum_i \phi_i(t)\, (exp\,(-dt/\tau_i) - 1)}{(1 - \sum_i \alpha_i)} \end{aligned} \tag{15}$$

Boundary conditions

$$\begin{aligned} \boldsymbol{J}_v|_{x=0^+} \cdot \boldsymbol{n} &= h_m\, c\, M_v\, \ln \left(\frac{1 - x_\infty}{1 - x_v|_{x=0}} \right) \\ \boldsymbol{J}_h|_{x=0^+} \cdot \boldsymbol{n} &= h_h\, (T|_{x=0} - T_\infty) \\ P_g|_{x=0^+} &= P_{atm} \end{aligned} \tag{16}$$

Table 4: List symbols (Latin letters)

Symbol	Name	Unit
a_w	sorption isotherm (water activity)	-
c	specific heat capacity	$J.kg^{-1}.K^{-1}$
D	diffusion coefficient	$m^2.s^{-1}$
f	dimensionless diffusion factor	-
h	specific enthalpy	$J.kg^{-1}$
h_h	heat transfer coefficient	$W.m^{-2}.K^{-1}$
h_m	mass transfer coefficient	$m.s^{-1}$
$\boldsymbol{j}_k$	diffusive flux of component k	$kg.m^{-2}; s^{-1}$
$\boldsymbol{J}_q$	heat flux	$W.m^{-2}$
$\boldsymbol{n}$	normal unit vector	-
T	temperature	K or $°C$
$\boldsymbol{v}$	general velocity vector	$m.s^{-1}$
X	solid moisture content (dry basis)	-
bold font	vector or tensor	

Table 5: List of symbols (Greek letters)

Symbol	Name	Unit
α	pre-exponential factor	-
ε	volume fraction	-
λ	thermal conductivity	$W.m^{-1}.K^{-1}$
φ	memory function	-
ω	mass fraction	-
ρ	density	$kg.m^{-3}$
τ	time constant	s
∂	partial derivative	-
∇	gradient	-
$\nabla\cdot$	divergence	-

Table 6: Subscripts and superscripts

Subscripts	**Meaning**
a	air
b	bound water
eff	effective property
eq	equilibrium
g	relative to the gaseous phase
v	water vapour
Superscript	**Meaning**
$\overline{\psi}$	averaged of variable ψ over the REV
$\overline{\psi}^{\ell}$	intrinsic average of ψ over phase ℓ